Journal of Applied Polymer Science

Crystallization, mechanical, and fracture behavior of mullite fiber-reinforced polypropylene nanocomposites

Muthukumaraswamy Ranagraj Vengatesan, Swati Singh, Vishnu V. Pillai, Vikas Mittal
Department of Chemical Engineering, The Petroleum Institute, Abu Dhabi, UAE
Correspondence to: V. Mittal; (E-mail: vmittal@pi.ac.ae)

ABSTRACT: This study describes the reinforcement effect of surface modified mullite fibers on the crystallization, thermal stability, and mechanical properties of polypropylene (PP). The nanocomposites were developed using polypropylene-grafted-maleic anhydride (PP-*g*-MA) as compatibilizer with different weight ratios (0.5, 1.0, 1.5, 2.5, 5.0, and 10.0 wt %) of amine functionalized mullite fibers (AMUF) via solution blending method. Chemical grafting of AMUF with PP-*g*-MA resulted in enhanced filler dispersion in the polymer as well as effective filler-polymer interactions. The dispersion of nanofiller in the polymer matrix was identified using scanning electron microscopy (SEM) elemental mapping and transmission electron microscopy (TEM) analysis. AMUF increased the Young's modulus of PP in the nanocomposites up to a 5 wt % filler content, however, at 10 wt % loading, a decrease in the modulus resulted due to agglomeration of AMUF. The impact strength of PP increased simultaneously with the modulus as a function of AMUF content (up to 5 wt %). The mechanical properties of PP-AMUF nanocomposites exhibited improved thermal performance as compared to pure PP matrix, thus, confirming the overall potential of the generated composites for a variety of structural applications. The mechanical properties of 5 wt % of AMUF filled PP nanocomposite were also compared with PP nanocomposites generated with unmodified MUF and the results confirmed superior mechanical properties on incorporation of modified filler. © 2016 Wiley Periodicals, Inc. J. Appl. Polym. Sci. **2016**, *133*, 43725.

KEYWORDS: composites; crystallization; mechanical properties; morphology; polyolefins

Received 2 November 2015; accepted 1 April 2016
DOI: 10.1002/app.43725

INTRODUCTION

Polymer nanocomposites are functional materials generated by reinforcing the polymers with a variety of nanofillers such as nanoparticles, nanorods, nanoplatelets, nanoflakes, nanofibers, etc. These materials offer superior mechanical, electrical, thermal, and gas barrier properties compared to that of pure polymer matrices due to nanoscale filler dispersion which leads to large number of interfacial contacts between the polymer and filler particles.[1] Among many polymers employed to generate polymer nanocomposites, significant research effort has been devoted to the development of polypropylene (PP) composites.[2–5] Main objective in developing PP nanocomposites has been to alleviate PP of its limitation of low impact resistance at low temperature while retaining tensile and thermal properties.[6] For instance, Zhao *et al.* studied the toughening mechanism of PP using alumina nanoparticles and impact fracture toughness of the PP increased by 25% on the addition of 1.5 wt % of alumina particles.[7] Peng *et al.* developed cellulose nanofibril reinforced PP nanocomposites, where the impact strength enhanced by 23% on addition of 1 wt % of cellolose nanofibril.[8] In another study, Bao *et al.* reported a balance in strength and toughness improvement by 100% of isotactic polypropylene (iPP) nanocomposites using surface functionalized graphene oxide.[2] Fuad *et al.* also studied the impact strength of PP/calcium carbonate ($CaCO_3$) nanocomposites generated using compatibilizer PP-graft-maleic anhydride (PP-*g*-MA). The authors concluded that addition of 5 wt % of $CaCO_3$ and 10 wt %of PP-*g*-MA resulted in an enhancement of impact strength by 77% as compared to pure PP.[9] Thus, the selection of suitable compatibilizers as well as nanomaterials are essential for the effective improvement of toughness behavior of PP while retaining its modulus and thermal stability.

Mullite is one of the ceramic nanomaterials with its structure combining silica and alumina ($3Al_2O_3{:}2SiO_2$) and is widely used in electronic, optical, and high-temperature structural materials.[10] In addition, mullite can be used in packaging materials and memory devices.[11,12] Recently, mullite fibers (MUF) have been used as nanofiller for the development of epoxy and unsaturated polyester resin nanocomposites due to high thermal stability, high oxygen resistance, and low dielectric constant.[13–16] To the best of our knowledge, no reports are available on the development of mullite fiber reinforced PP nanocomposites. In

this work, the effect of amine functionalized mullite fibers (AMUF) on the crystallization, thermal stability, and mechanical properties of PP is reported. The goal was to generate functional composite materials with simultaneous enhancement of modulus and impact properties.

EXPERIMENTAL

Materials

Aluminium nitrate nonhydrate, aluminium isopropxide, tetraethoxyorthosilicate (TEOS), aminopropyltriethoxysilane (APTES), PP-*g*-MA ($M_w \sim$ 9,100 and maleic anhydride grafting % of 8–10) and solvents were procured from Sigma Aldrich and were used without purification. Isotactic PP (HD51CF) was received from Abu Dhabi Polymers (Borouge), UAE.

Synthesis of Mullite Fibers (MUF) and Amine Functionalization (AMUF)

Synthesis of mullite fiber was performed as per the reported literature.[14] In brief, 27.09 g (0.0773 mol) of aluminum nitrate nonhydrate was dissolved in 144 mL of deionized (DI) water at 30 °C. Subsequently 14.7 g (0.0719 mol) of aluminum isopropoxide and 10.0 g (0.048 mol) of TEOS were added simultaneously at 30 °C. The mixture was stirred for 24 h at 30 °C. The solution was transferred into a ceramic bowl and the contents were aged for 48 h at 50 °C, followed by 24 h at 90 °C. After aging, the solution transformed into gel form, which was calcinated at 1200 °C for 120 min with a heating rate of 5 °C/min. The calcinated material was ball milled for 60 min at 1000 rpm to obtain MUF. The as-obtained MUF materials was amine functionalized using APTES. For this, 5 g of MUF was dispersed in 350 mL of anhydrous ethanol using an ultra-sonication bath for 1 h at 30 °C. Subsequently, 50 g of APTES was added to the MUF dispersion. The mixture was refluxed for 16 h and centrifuged, followed by washing using ethanol. The resulting AMUF was dried under vacuum for 8 h at 50 °C.

Preparation of PP-AMUF Nanocomposites

Totally, 50 mg of AMUF (0.5 wt %) was dispersed in 400 mL of *o*-xylene using an ultra-sonication bath at 30 °C for 1 h. Subsequently 9.45 g of PP and 0.5 g of PP-*g*-MA were added to the dispersion. The mixture was stirred for 2 h at 130 °C and the solvent was evaporated at 80 °C in vacuum. The resulting hybrid sample (PP-AMUF1) was processed using injection molding (Thermo Scientific) at 190 °C with 400 bar for 10 s. Similarly, a series of PP-AMUF composites were prepared by varying the content of AMUF as 1.0, 1.5, 2.5, 5.0, and 10.0 wt %. The amount of PP-*g*-MA was fixed to 5 wt % in all the composites. The nanocomposites were, thus, designated as PP-AMUF2 (1.0 wt % AMUF), PP-AMUF3 (1.5 wt % AMUF), PP-AMUF4 (2.5 wt % AMUF), PP-AMUF5 (5.0 wt % AMUF), and PP-AMUF6 (10.0 wt % AMUF). PP nanocomposite with 5 wt % of unmodified mullite (MUF) was also generated using the above procedure using 5 wt % PP-*g*-MA. A hybrid of PP-*g*-MA and AMUF was also generated to confirm the chemical reaction between the two. For this, 0.2 g of AMUF was dispersed in 20 mL of *o*-xylene using an ultra-sonication bath at 30 °C for 1 h. Subsequently, 0.2 g of PP-*g*-MA was added to the dispersion and the mixture was stirred for 2 h at 130 °C. This was followed by evaporation of the solvent under vacuum at 80 °C.

Characterization

IR spectra of the PP-*g*-MA and PP-*g*-MA-AMUF hybrid were collected on Nicolet iS10 spectrometer equipped with SmartiTR diamond ATR accessory (angle of incidence of 45°), DTGS KBr detector and KBr beam splitter. It had a diamond ATR crystal (index of refraction = 2.4 at 1000 cm^{-1}) and a depth permeation of 2 μm at 1000 cm^{-1} for sample with refractive index of 1.5. The spectra of the samples were recorded using OMNIC software in the spectral range of 4000–600 cm^{-1} with a resolution of 4 cm^{-1} from 32 scans. Thermal properties of the PP-AMUF composites were recorded using TA Discovery thermogravimetric analyzer (TGA) in nitrogen medium. The temperature range was 35–700 °C and a heating rate of 10 °C/min was used. Differential scanning calorimetric (DSC) analysis of the composites was performed on a TA Discovery DSC under nitrogen atmosphere. 5–7 mg of the sample weight was used for both DSC and TGA analysis. The scans were obtained from 35 to 200 °C using a heating rate of 10 °C/min. The second heating runs were carried out in the same temperature range and were used for calculation of the crystallinity. Tensile analysis of the PP-AMUF composites was carried out using universal testing machine (Instron, USA) (ASTM D 638). The dumbbell-shaped samples were used. A loading rate of 10 mm/min was used and the tests were carried out at room temperature. The tensile strength and modulus of the composites were calculated using Win Test Analysis software. An average of five sample values was reported. Un-notched impact strength of nanocomposites was measured using Resil Impactor (from Ceast) with hammer energy of 4 J and speed 3.46 m/s according to ASTM D256. The test was conducted at room temperature and rectangular bar shaped samples were used. Izod impact strength for each nanocomposite sample represented the average from five test specimens. Wide-angle X-ray diffraction (WAXRD) analysis of the filler and composites was performed on an analytical powder diffractometer (X'Pert PRO) using CuKα radiation (λ = 1.5406 Å) in reflection mode. A zero-background holder was used to minimize the noise. The samples were step-scanned from 2θ = 5-60° at room temperature using a step size of 2θ = 0.02° and a step time of 10 s. The morphology of AMUF fibers and the dispersion of AMUF in PP nanocomposites were examined in a transmission electron microscope (FEI, TECNAI) at 200 kV without staining. The morphology of AMUF was studied by dispersing the sample in ethanol; then the suspended particles were transferred to 400 mesh copper grids (coated with holey carbon film). The dispersion of AMUF and MUF in PP nanocomposites was studied by microtoming ultrathin sections in the range of 30-70 nm using a PowerTome equipped with a diamond knife at −6 °C. The sections were collected on 400 mesh formvar electron microscopy grids (coated with copper) and were subsequently examined in a FEI electron microscope (TECNAI) at 200 kV at room temperature without staining. TEM image processing was performed using Digital Micrograph software (Gatan, USA). The microstructure of the fracture surface of the nanocomposites was analyzed using scanning electron microscope (SEM) (FEI Quanta, FEG250, USA) with elemental mapping at accelerating voltages of 10–20 kV. The sample surfaces were sputter-coated with 3 nm thick gold layer.

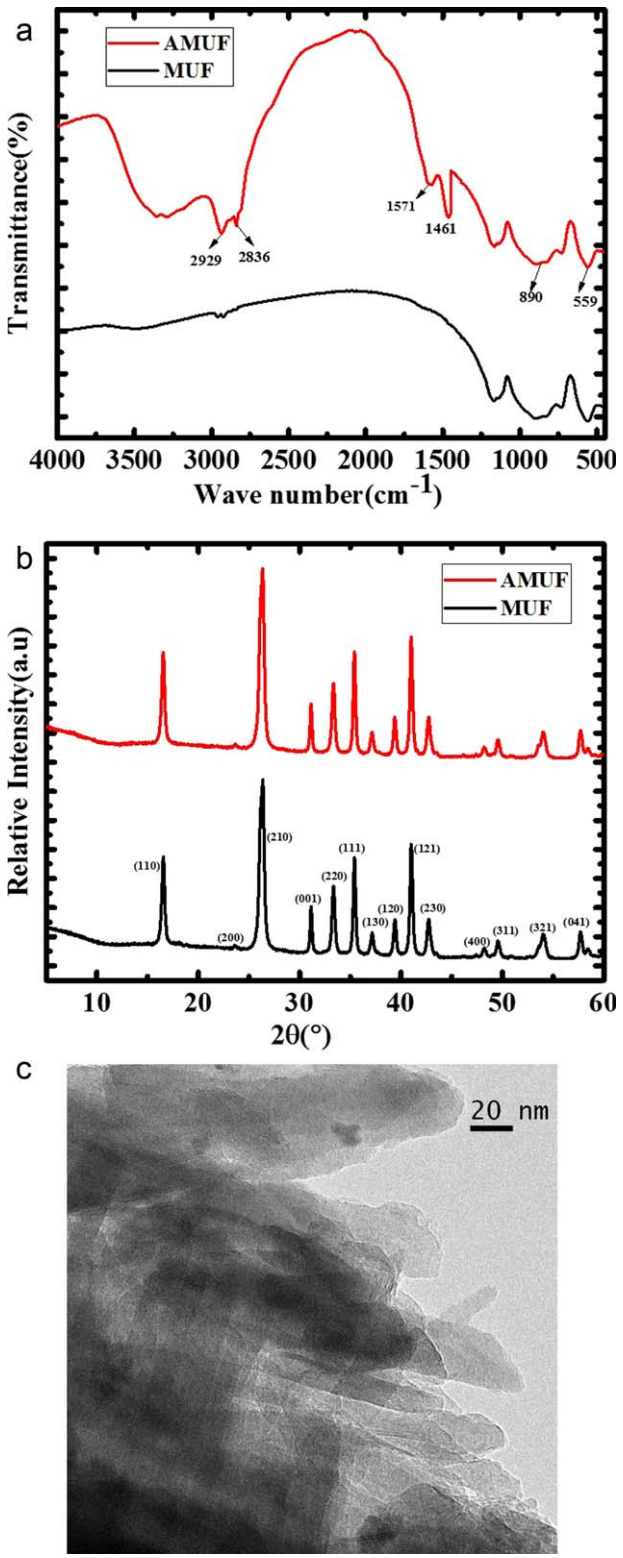

Figure 1. (a) FTIR spectra of MUF and AMUF fibers, (b) XRD of MUF and AMUF, (c) high resolution TEM micrograph of AMUF fibers. [Color figure can be viewed in the online issue, which is available at wileyonlinelibrary.com.]

RESULTS AND DISCUSSION

Figure 1(a) shows the FTIR spectra of unmodified mullite (MUF) and amine functionalized mullite fiber (AMUF). After grafting of MUF with APTES, new peaks appeared at 2929 cm^{-1} and 2836 cm^{-1} representing the characteristic $–CH_2$ stretching vibrations in AMUF. The appearance of a band at 1461 cm^{-1} resulted due to $–CH_2$ bending (scissoring) vibration of the silylated alkyl chains in AMUF. The band at 1567 cm^{-1} corresponded to N—H bending (scissoring) of the amine group in AMUF. This indicated the successful surface modification of MUF with APTES. In addition, the broad peaks at 890 cm^{-1} and 559 cm^{-1} represented the —Si—O—Al— and Al—O— stretching of the mullite fibers, respectively. Figure 1(b) shows the XRD spectra of MUF and AMUF. The X-ray diffraction peaks in MUF perfectly matched with the orthorhombic mullite structure. After functionalization, there was no change in the diffraction pattern which indicated that the surface functionalization did not alter the crystallinity of the MUF. Figure 1(c) also shows the high-resolution TEM micrograph of AMUF. It represented a well-ordered one dimensional (1D) fibrous rod like structure at nanoscale level. The average aspect ratio of AMUF was 4.5 which was calculated as the ratio between the average length (87.0 nm) and diameter (19.5 nm) of AMUF. Figure 2 shows the FTIR spectra of PP-*g*-MA and PP-*g*-MA-AMUF hybrid. The peaks at 1776 cm^{-1} and 1707 cm^{-1} in the PP-*g*-MA spectrum were attributed to the C=O stretching of anhydride and carboxylic acid groups, respectively. A covalent binding between the maleic anhydride and amine groups of MUF was successfully achieved as the intensity of both 1776 cm^{-1} and 1707 cm^{-1} peaks diminished in PP-*g*-MA-AMUF hybrid. In addition, a new peak at 1694 cm^{-1} was observed in the hybrid, which represented the characteristic peak of the imide group.[17] Broad peak also appeared at 1004 cm^{-1} indicating the —Si—O—Si— linkage along with a peak at 647 cm^{-1} representing the stretching frequency of Al—O linkage.

Figure 3 demonstrates the melting and crystallization curves of pure PP and PP-AMUF nanocomposites. The percentage of

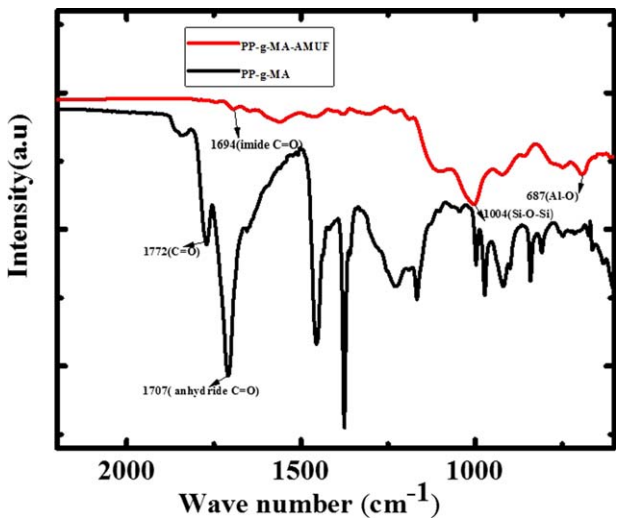

Figure 2. FTIR spectra of PP-*g*-MA and PP-*g*-MA-AMUF hybrid. [Color figure can be viewed in the online issue, which is available at wileyonlinelibrary.com.]

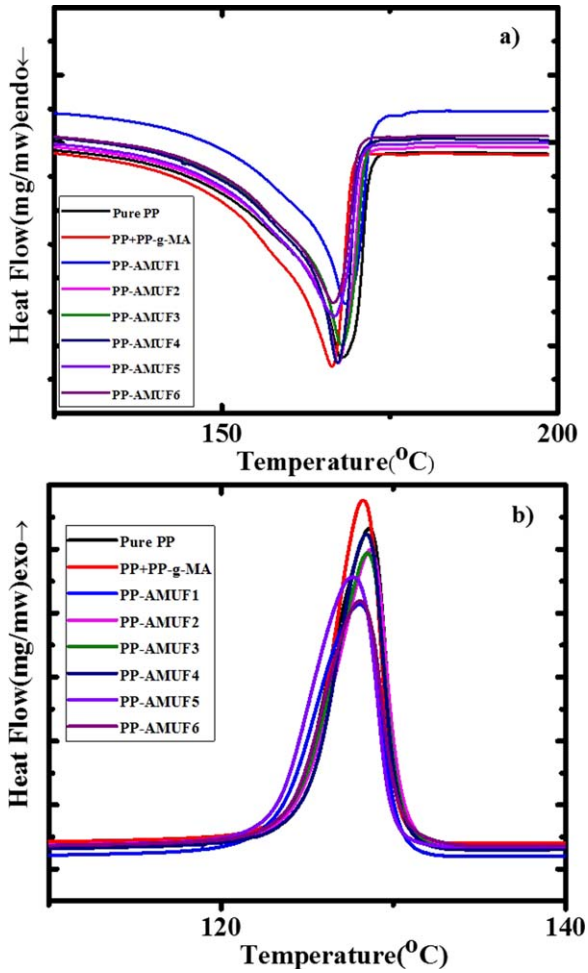

Figure 3. (a) Melting endotherms and (b) crystallization exotherms of PP and PP-AMUF nanocomposites. [Color figure can be viewed in the online issue, which is available at wileyonlinelibrary.com.]

crystallinity value of PP nanocomposites was calculated by the following eq. (1) and the values are presented in Table I.[18]

$$\text{Xc}\ (\%) = \frac{\Delta H_m}{(1-f)\Delta H_m^o} \times 100 \qquad (1)$$

Where X_c is the percentage crystallinity, ΔH_m is the melting enthalpy of the polymer (second heating cycle) and ΔH_m^o is the

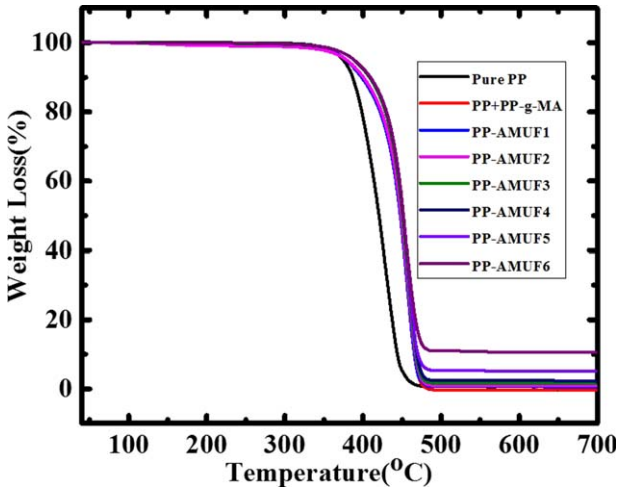

Figure 4. TGA thermograms of PP and PP-AMUF composites. [Color figure can be viewed in the online issue, which is available at wileyonlinelibrary.com.]

melt enthalpy of 100% crystalline PP, taken as 209 J/g.[19] Addition of 5 wt % of PP-*g*-MA to PP did not change the crystallinity of the polymer. Addition of AMUF slightly increased the crystallinity of the PP matrix up to 5 wt %, whereas further increase of its content resulted in a decrease in crystallinity. For instance, the ΔH_m value of pure PP was 93.15 J/g, which was decreased to 80.6 J/g for the PP composite with 10 wt % AMUF. The higher filler content probably resulted in enhanced degree of filler agglomeration in PP matrix, which hindered the crystallization of PP chains. In addition, no significant change in the T_c and T_m of the polymer was observed in the nanocomposites.

Figure 4 shows the TGA thermograms of PP and PP-AMUF nanocomposites. The thermal degradation temperature for 10 and 40% weight loss as well as char yield value at 700 °C are also presented in Table II. Thermal degradation temperature for 10 and 40% weight loss in the nanocomposites increased with enhancement of filler fraction up to 1.5 wt %. Beyond 1.5 wt %, similar degradation temperatures were observed. This indicated that the nanocomposites were thermally stable as compared to pure PP. The improved thermal stability of PP-AMUF

Table I. Calorimetric Behavior of PP and PP-AMUF Composites

Sample	T_m (°C)	ΔH_m (J/g)	T_c (°C)	ΔH_c (J/g)	X_c (%)
Pure PP	167.1	93.2	128.3	98.2	–
PP+PP-g-MA	166.1	93.1	127.6	98.4	–
PP-AMUF1	168.2	93.6	128.1	93.3	45.2
PP-AMUF2	167.1	96.2	128.7	98.5	46.5
PP-AMUF3	167.6	96.5	128.6	96.9	46.9
PP-AMUF4	167.4	95.8	128.2	94.8	47.0
PP-AMUF5	166.4	94.5	127.7	94.5	47.6
PP-AMUF6	166.2	80.6	128.3	82.9	42.8

Table II. Thermal Stability and Char Yield of PP and PP-AMUF Composites

Sample	T_{10}^d (°C)	T_{40}^d (°C)	Char yield at 700 °C (%)
Pure PP	386	414	0.00
PP+5 wt % PP-g-MA	398	442	0.00
PP-AMUF1	398	444	0.55
PP-AMUF2	400	444	0.94
PP-AMUF3	408	446	1.50
PP-AMUF4	409	447	2.12
PP-AMUF5	409	447	5.24
PP-AMUF6	409	447	10.41

Table III. Mechanical Properties of PP and PP-AMUF Composites

Sample	Tensile modulus (MPa)	Tensile stress at yield (MPa)	Elongation at break (%)	Un-notched izod impact strength (KJ/m^2)
Pure PP	826.1 (±10)	37.5 (±2)	23.4 (±2)	7.2 (±0.5)
PP+5 wt % PP-*g*-MA	833.0 (±10)	36.6 (±2)	28.9 (±2)	9.4 (±0.5)
PP-AMUF1	847.4 (±10)	36.7 (±2)	28.1 (±2)	12.6 (±0.5)
PP-AMUF2	856.1 (±10)	35.7 (±2)	18.6 (±2)	14.3 (±0.5)
PP-AMUF3	938.8 (±10)	35.1 (±2)	15.7 (±2)	16.7 (±0.5)
PP-AMUF4	1034.1 (±10)	34.8 (±2)	18.1 (±2)	22.1 (±0.5)
PP-AMUF5	1081.3 (±10)	34.3 (±2)	15.6 (±2)	28.3 (±0.5)
PP-AMUF6	928.7 (±10)	33.6 (±2)	12.1 (±2)	8.5 (±0.5)

nanocomposites may be attributed to the adsorption of the volatile decomposition products generated during the thermal degradation on the surface of AMUF fibers, thereby, resulting in delayed degradation of the PP matrix. Similar findings for mullite reinforced epoxy and polyester nanocomposites have also been reported earlier.[14,15] The char yield of the nanocomposites increased with increase in AMUF content. For example, PP-AMUF6 had the char yield of 10.2% as compared to 0% for pure PP at 700 °C in nitrogen atmosphere. It is well know that the mullite, due to structural combination of alumina and silica, acts as a high temperature insulator and hinders the diffusion of low molecular weight volatiles within the PP-AMUF nanocomposites.[14]

The influence of AMUF on the tensile performance of PP is reported in Table III. It was expected that the surface modification of MUF along with the compatibilizer would result in improved interfacial interactions between the polymer and filler particles. The tensile modulus in the nanocomposites increased with increasing AMUF content up to 5 wt %. For instance, the tensile modulus of pure PP was 826 MPa, which was enhanced by >30% in the composite with 5 wt % AMUF. In other words, the nanofibers endured more load during the tensile test due to efficient stress transfer from the polymer chains, thereby yielding nanocomposites with high stiffness. As mentioned earlier, strong interfacial interactions between the polymer and amine functionalized filler resulted in efficient load transfer between the PP matrix and the nanofiller.[20] Covalent bonding of the amine functionalized fibers with the PP-*g*-MA would have resulted in the enhanced plastic deformation. Such bonding would also result in uniform distribution of filler in the polymer, thereby, further enhancing the modulus of the polymer.[21] At a higher loading of 10 wt % of AMUF, the modulus of the nanocomposite decreased probably due to filler agglomeration, which was also earlier indicated by the calorimetric studies. Due to the characteristic of AMUF fibers exhibiting a solid-state plasticizer behavior in the nanocomposites, the tensile strength of the composites did not deteriorate significantly and nearly 8% reduction was observed for the composite with 5 wt % AMUF content.

The impact behavior of the nanocomposites was studied at room temperature using un-notched samples and the results are illustrated in Table III. The impact strength of the nanocomposites enhanced with increase in the filler content up to 5 wt %. From a value of 7.15 KJ/m^2 for pure PP, the composite with 5

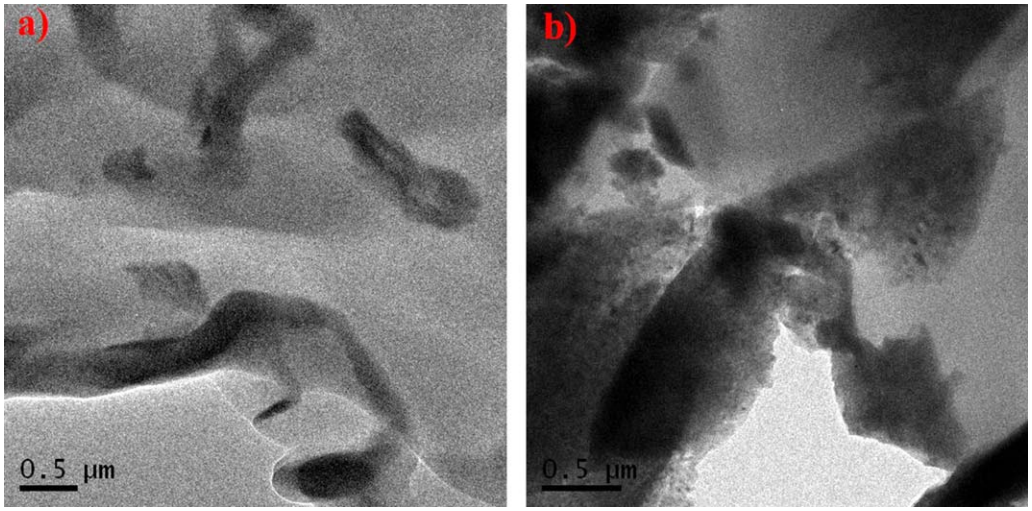

Figure 5. TEM images of (a) 5 wt % AMUF filled PP nanocomposite (PP-AMUF5), (b) 5 wt % unmodified MUF filled PP nanocomposite. [Color figure can be viewed in the online issue, which is available at wileyonlinelibrary.com.]

Table IV. Comparative Mechanical Properties of PP-AMUF Nanocomposites with Other PP Nanocomposites

Nanocomposites	Nanofiller content (wt %)	Young's Modulus (MPa)	Impact strength (KJ/m^2)
Polypropylene/nano silica	2.5,[26] 5.0[27]	1620,[26] 1095[27]	33,[26] 5.5[27]
PP/graphene nanocomposite	0.5[28]	1750[28]	4[28]
PP/alumina	1.5[7]	1730[7]	3.5[7]
PP/organoclay	10,[29] 4[30]	936,[29] 830[30]	20.3,[29] 3.2[30]
PP/MWCNT	0.5[31]	890[31]	18.5[31]
PP/natural fibers	30,[32] 6[33]	1700,[32] 1940[33]	4.5,[32] 3.8[33]
PP/glass fibers	23.1[33]	4150[33]	11.69[33]
PP/CaCO3	15,[34] 10[35]	800,[34] 740[35]	25,[34] 25.9[35]
PP/mullite fiber (present work)	5	1081	28.3

wt % AMUF content exhibited the impact strength of 28.32 KJ/m^2. This was significant as it confirmed the simultaneous enhancement of modulus and impact strength of PP with AMUF fibers. The major deformation mechanisms such crazing and shear yielding plays a vital role in the fracture toughness of the semi crystalline PP based nanocomposites. For the PP nanocomposites, the fading and micro cracking mechanism were found to be dominant in the impact performance. The strong

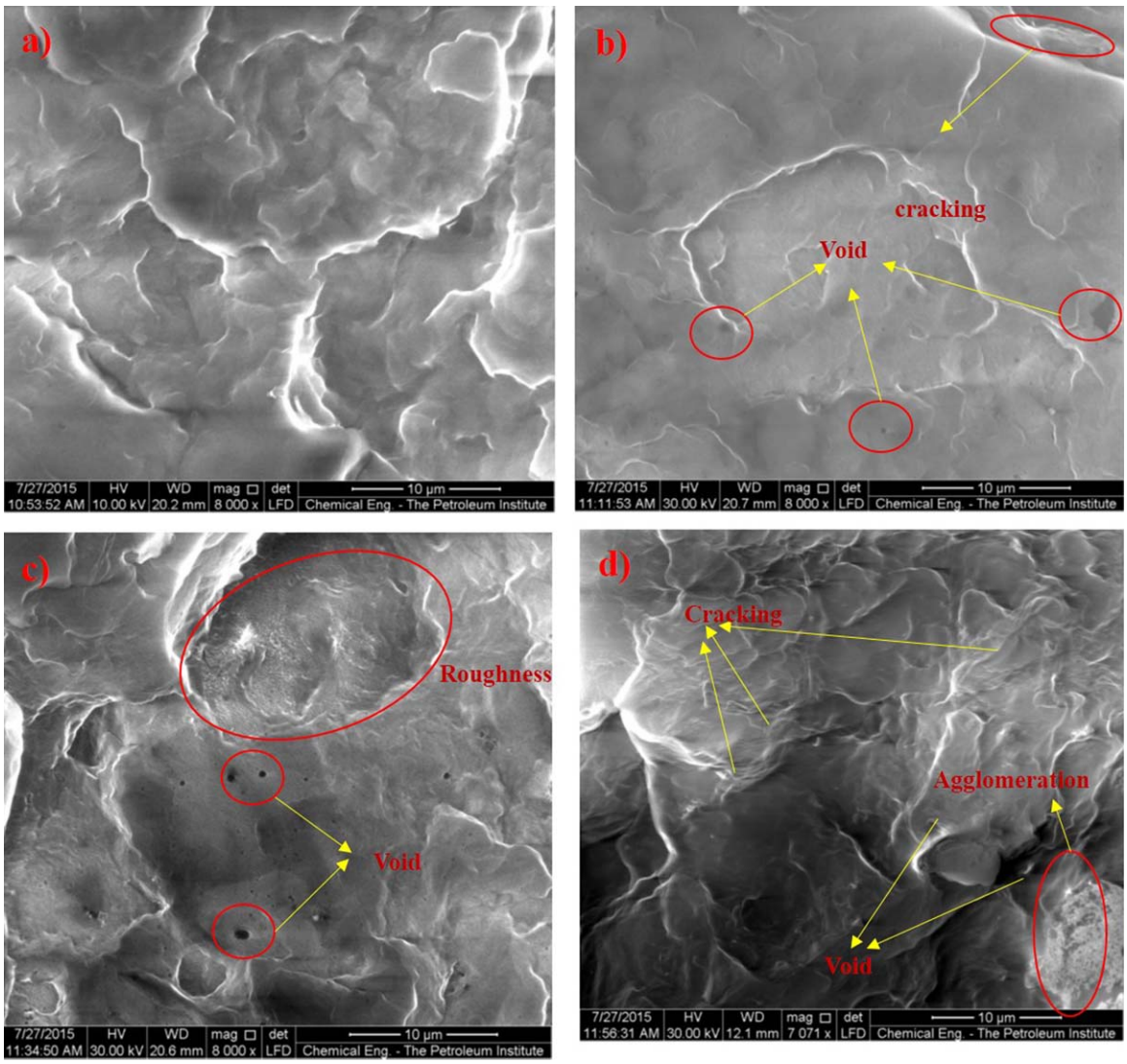

Figure 6. SEM images of fracture surface of (a) pure PP, (b) PP-AMUF2, (c) PP-AMUF5 and (d) PP-AMUF6. [Color figure can be viewed in the online issue, which is available at wileyonlinelibrary.com.]

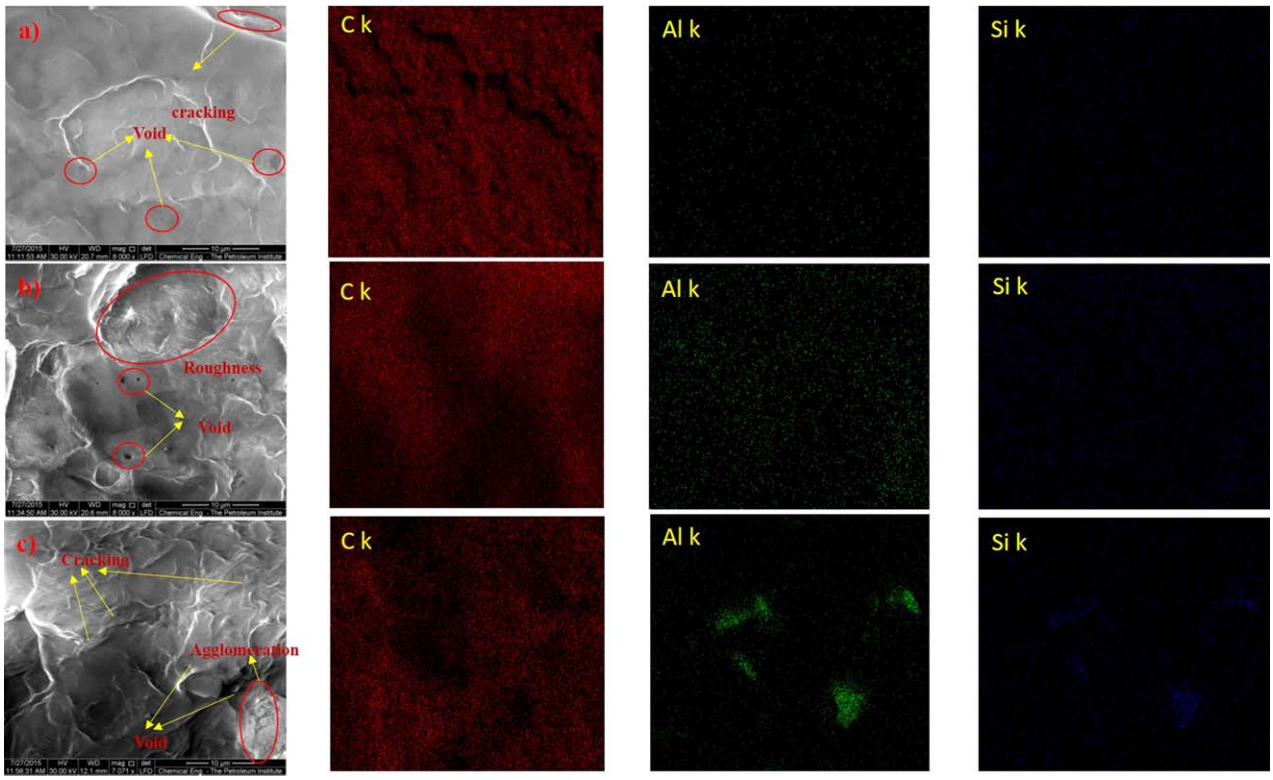

Figure 7. SEM elemental mapping of fracture surface of (a) PP-AMUF2, (b) PP-AMUF5 and PP-AMUF6. [Color figure can be viewed in the online issue, which is available at wileyonlinelibrary.com.]

interfacial adhesion of the surface modified nanofiller reduced the growth of micro cracks in the nanocomposites.[22] In the case of unmodified nanofiller reinforced nanocomposites, the interfacial adhesion was poor and the nanoparticles are easily agglomerated in the polymer matrix which released stress from the crack tip, thus, enhancing the growth of micro voids in the matrix.[23–25] It is well known that the surface modified nanofiller possesses better interfacial adhesion in the polymer matrix in comparison to that of the unmodified nanofiller. Therefore, the AMUF reduced the growth of micro voids in the nanocomposites, and observed more plastic deformation in the PP/AMUF nanocomposites. It also indicated that the amine modified MUF was dispersed uniformly at nanoscale level within the PP matrix, which subsequently reduced the size of void dimension and major crack formation.[22] Similar to the tensile properties, further increase in the filler content to 10 wt % resulted in significant deterioration of impact performance.

In order to further confirm the influence of interfacial adhesion between nanofiller and PP matrix, mechanical properties of the 5 wt % AMUF filled PP nanocomposite were compared with PP nanocomposite generated with 5 wt % unmodified MUF. The AMUF filled PP nanocomposite exhibited Young's modulus and impact strength of 1081 MPa and 28.3 KJ/m^2, respectively. However, the MUF filled PP nanocomposite has the Young's modulus and impact strength of 931 MPa and 13.8 KJ/m^2, respectively. This indicated that the AMUF possessed better interfacial adhesion compared to that of unmodified MUF. Figure 5(a,b) also represent the TEM images of 5 wt % AMUF and MUF filled PP nanocomposites, respectively. From the TEM analysis, it was observed that AMUF was finely dispersed in the PP matrix with a fibroid morphology [Figure 5(a)], however, unmodified MUF exhibited agglomeration in the PP matrix [Figure 5(b)]. The impact and modulus value of the PP-AMUF nanocomposite has been compared with different types of the PP nanocomposites and presented in Table IV.[7,8,26–35] As expected, the property values for each nanocomposite differed from others due to a variety of factors such as preparation methods, type of nanofillers, interfacial adhesion, filler fraction, filler dimensions, test conditions, etc. Thus, though it is not easy to draw a coherent comparison of impact and modulus of the present work with other nanocomposites, nonetheless, improved degree of property enhancement can still be envisaged for these composites.

To gain further insights into the morphology of the composites, surface analysis of the fracture surfaces was carried out. Figure 6 shows the SEM images of the fracture surface of the PP matrix and PP-AMUF nanocomposites. In Figure 6(a) for pure PP, a smooth fracture surface was observed. The fracture surface in Figure 6(b) and c exhibited a plastic deformation during the Izod impact test. The voids and cracks were minimal in these 1 wt % and 5 wt % AMUF-filled PP nanocomposites. These results suggested that covalently bound AMUF along with its uniform dispersion provided dissipation of large amount of energy, thus, leading to high toughness of the PP nanocomposites. On the other hand, the fractography of 10 wt % AMUF filled PP nanocomposite exhibited a large number of voids,

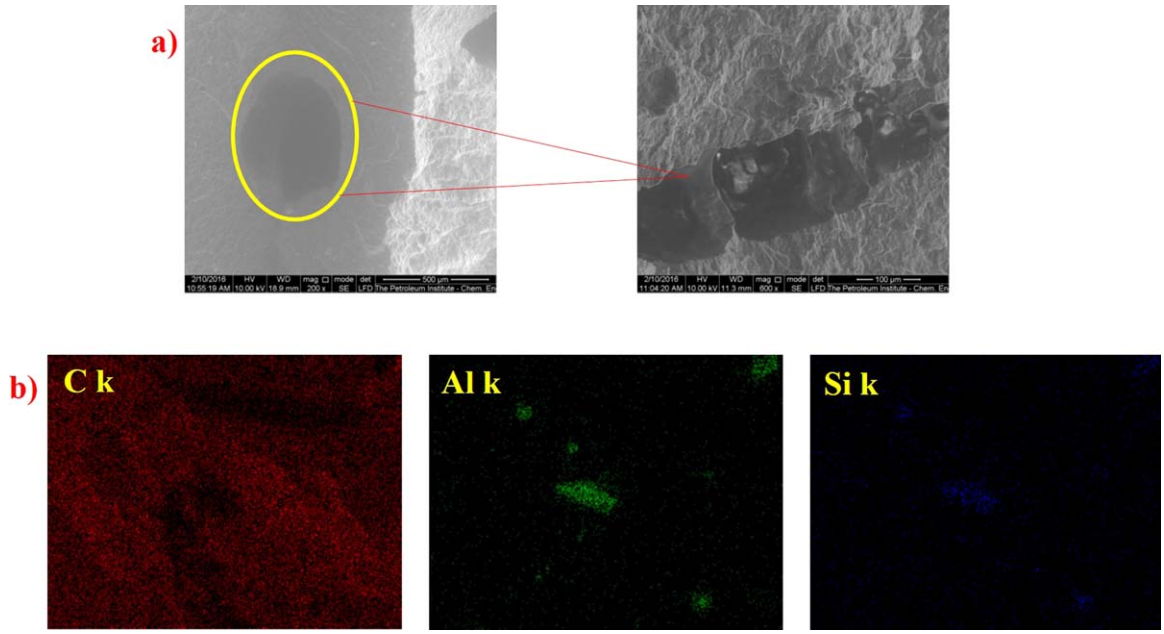

Figure 8. (a) SEM image and (b) elemental mapping for 5 wt % unmodified MUF filled PP nanocomposite. [Color figure can be viewed in the online issue, which is available at wileyonlinelibrary.com.]

agglomeration, and cracking [Figure 5(d)]. As mentioned earlier, this behavior resulted from the aggregation of AMUF within the PP matrix which was also evidenced by the SEM elemental mapping in Figure 7. The elemental mapping was used to study the dispersion of nanofiller in the bulk PP matrix. As the nanofiller contained the major elements such as Al and Si, then the distribution of these elements provided the information about dispersion level of the nanofiller in the bulk PP. Figure 7(a–c) represent the SEM elemental mapping of 1, 5, and 10 wt % of AMUF filled PP nanocomposites respectively. It was observed that for the nanocomposites up to 5 wt % of AMUF, the nanofiber dispersed uniformly into the PP without delamination. In the case of 10 wt % filled nanocomposites, the distribution of elements was not uniform and resulted in agglomeration of AMUF in the bulk PP [Figure 7(c)]. Thus, the aggregation of AMUF at higher filler content in the composites reduced the interfacial interaction between the polymer and fibers. This produced stress concentration regions, which required less energy for crack propagation, thus, resulting in low impact strength.[36] The fractured surface of 5 wt % unmodified MUF filled PP nanocomposite is also presented in Figure 8(a) and the respective elemental mapping is shown in Figure 8(b). The composite exhibited large voids at the fractured surface which resulted in low impact strength and also the elemental mapping resulted the agglomeration of MUF in the PP nanocomposite.

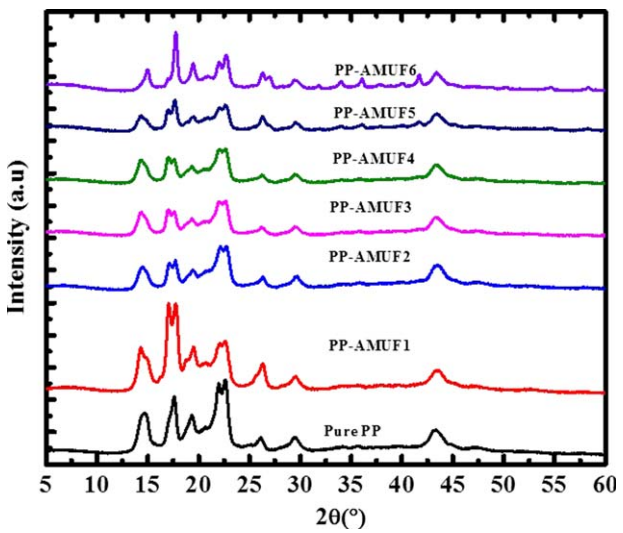

Figure 9. XRD analysis of PP and PP-AMUF composites. [Color figure can be viewed in the online issue, which is available at wileyonlinelibrary.com.]

The XRD spectra of pure PP and PP-AMUF nanocomposites are represented in Figure 9. The diffractograms of pure PP exhibited five distinct crystalline peaks at 2θ values of ~14.5°, 17.5°, 19.3°, 22.0°, and 22.7°. No β and γ phases were observed in both pure PP and PP-AMUF nanocomposites. In the XRD spectra of PP nanocomposites, a shoulder peak at 17.5° was observed due to the addition of AMUF. This suggested that the plane (040) contained different crystal structures in the polymer nanocomposites and the relative intensity of the peaks at (040) increased with increase in AMUF content. Therefore, it can be confirmed that AMUF helped in nucleation of PP crystallites preferably in (040) plane.[37]

CONCLUSIONS

In the current study, mullite fibers were successfully generated and surface modified with amine functional groups. The functionalized mullite could be used as a functional filler to generate PP nanocomposites, in the presence of PP-*g*-MA. AMUF resulted in chemical interactions with PP-*g*-MA, which,

translated in an enhancement in the polymer-fiber interfacial interactions and improved thermal and mechanical properties of the resulting composites. The thermal stability and char yield in the composites increased with enhancing the filler content. Addition of AMUF simultaneously increased the Young's modulus and impact strength of PP up to 5 wt % filler content. Incorporation of AMUF marginally increased the crystallinity of the PP and acted as a weak nucleating agent. The SEM analysis of fracture surface of the PP-AMUF nanocomposites revealed lower extent of cracking and void up to 5 wt % of AMUF content, resulting due to the better filler dispersion which helped the polymer to dissipate large amount of impact energy. The molecular level dispersion of mullite in the PP matrix, studied using TEM, SEM elemental mapping, revealed homogenous dispersion of AMUF in the PP matrix up to 5 wt % filler content. Due to the optimal enhancement of properties of the developed PP-AMUF nanocomposites, these materials represent high potential for their application in engineering sectors.

ACKNOWLEDGMENTS

The authors sincerely thank the PI Research Centre, The Petroleum Institute for the financial support. The authors also thank Mr. Anish Varghese, Mrs. Anjana and Mrs. Sabna for carrying out the impact, XRD and SEM analysis. The authors specially thank Mr. Samuel Stephen for helping in the TEM analysis.

REFERENCES

1. Vengatesan, M. R.; Mittal, V. Surface Modification of Nanoparticle and Natural Fiber Fillers; Wiley: New York, **2015**, Chapter 1, p 1.
2. Bao, R. Y.; Cao, J.; Liu, Z. Y.; Yang, W.; Xie, B. H.; Yang, M. B. *J. Mater. Chem. A* **2014**, *2*, 3190.
3. Chandramouleeswaran, S.; Mhaske, S. T.; Kathe, A. A.; Varadarajan, P. V.; Prasad, V.; Vigneshwaran, N. *Nanotechnology* **2007**, *18*, 385702.
4. Du, H.; Zhang, Y.; Liu, H.; Liu, K.; Jin, M.; Li, X.; Zhang, J. *Polymer* **2014**, *55*, 5001.
5. Zhang, Z.; Wang, C.; Meng, Y.; Mai, K. *Compos. A* **2012**, *43*, 189.
6. Lin, Y.; Chen, H.; Chan, C. M.; Wu, J. *Macromolecules* **2008**, *41*, 9204.
7. Zhao, H.; Li, R. K. Y. *J. Polym. Sci. Part B. Polym. Phy.* **2005**, *43*, 3652.
8. Peng, Y.; Gallegos, S. A.; Gardner, D. J.; Han, Y.; Cai, Z. *Polym. Compos.* **2016**, *37*, 782.
9. Fuad, M. Y. A.; Hanim, H.; Zarina, R.; Ishak, Z. A. M.; Hassan, A. *eXPRESS Polym. Lett.* **2010**, *4*, 611.
10. Zhang, B.; Cao, C.; Xiang, X.; Zhu, H. *Chem. Comm.* **2004**, 2452.
11. Barnwal, R.; Villar, M. P.; Garcia, R.; Laine, M. *J. Am. Ceram. Soc.* **2001**, *84*, 951.
12. Tummala, R. R. *J. Am. Ceram. Soc.* **1991**, *74*, 895.
13. Kanimozhi, K.; Prabunathan, P.; Selvaraj, V.; Alagar, M. *High Perform. Polym.* **2014**, *18*, 1.
14. Kanimozhi, K.; Devaraju, S.; Vengatesan, M. R.; Selvaraj, V.; Alagar, M. *High Perform. Polym.* **2013**, *25*, 658.
15. Kanimozhi, K.; Prabunathan, P.; Selvaraj, V.; Alagar, M. *Polym Compos.* **2014**, *35*, 1663.
16. Kanimozhi, K.; Prabunathan, P.; Selvaraj, V.; Alagar, M. *Polym. Bull.* **2014**, *71*, 1277.
17. Tambe, P. B.; Bhattacharyya, A. R.; Kamath, S. S.; Kulkarni, A. R.; Sreekumar, T. V.; Srivastav, A.; Rao, K. U. B.; Liu, Y.; Kumar, S. *Polym. Eng. Sci.* **2012**, *52*, 1183.
18. Chafidz, A.; Kaavessina, M.; Zahrani, S. A.; Otaibi, M. N. A. *J. Polym. Res.* **2014**, *21*, 483.
19. Pedrazzoli, D.; Khumalo, V. M.; Kocsis, J. K.; Pegoretti, A. *Polym. Test.* **2014**, *35*, 92.
20. Qian, D.; Dickey, E. C.; Andrews, R.; Rantell, T. *Appl. Phys. Lett.* **2000**, *76*, 2868.
21. Mandhakini, M.; Chandramohan, A.; Vengatesan, M. R.; Alagar, M. *High Perform. Polym.* **2011**, *23*, 403.
22. Liang, J. Z.; Li, R. K. Y. *J. Appl. Polym. Sci.* **2000**, *77*, 409.
23. Wei, G. X.; Sue, H. *J. Polym. Eng. Sci.* **2000**, *40*, 1979.
24. Jang, B. Z.; Uhlmann, D. R.; Vander Sande, J. B. *J. Appl. Polym. Sci.* **1985**, *30*, 2485.
25. Zebarjad, S. M. *Mater. Des.* **2003**, *24*, 531.
26. Bikiaris, D. N.; Vassiliou, A.; Pavlidou, E.; Karayannidis, G. P. *Eur. Polym. J.* **2005**, *41*, 1965.
27. Panaitescu, D. M.; Vuluga, Z.; ; Radovici, C.; Nicolae, C. *Polym. Test.* **2012**, *31*, 355.
28. Shokrieh, M. M.; Joneidi, V. A. *J. Compos. Mater.* **2015**, *49*, 2317.
29. Sanporean, (ńee Potarniche), C. G.; Vuluga, Z.; Radovici, C.; Panaitescu, D. M.; Iorga, M.; Christiansena, J. D.; Mosca, A. *RSC Adv.* **2014**, *4*, 6573.
30. Yuana, Q.; Misra, R. D. K. *Polymer* **2006**, *47*, 4421.
31. Wang, Z. J.; Kwon, D. J.; Gu, G. Y.; Kim, H. S.; Kim, D. S.; Lee, C. S.; DeVries, K. L.; Park, J. M. *Compos. Sci. Technol.* **2013**, *81*, 69.
32. Kamardin, N. K.; Taib, Y. M.; Kalam, A. *Appl. Mech. Mater.* **2013**, *393*, 152.
33. Tjonga, S. C.; Xua, S. A.; Lia, R. K. Y.; Mai, Y. W. *Compos. Sci. Technol.* **2002**, *62*, 831.
34. Dasari, A.; Zhang, Q. X.; Yu, Z. Z.; Mai, Y. W. *Macromolecules* **2010**, *43*, 5734.
35. Wang, Y.; Shen, H.; Li, G.; Mai, K. *J. Appl. Polym. Sci* **2009**, *113*, 1584.
36. Karmakar, A.; Chauhan, S. S.; Modak, J. M. *Comp A* **2007**, *38*, 227.
37. Mittal, V.; Luckachan, G. E.; Matsko, N. B. *Macromol. Chem. Phys.* **2014**, *215*, 255.